NANO LETTERS

Letter

pubs.acs.org/NanoLett

Nanovoid Formation and Annihilation in Gallium Nanodroplets under Lithiation–Delithiation Cycling

Wentao Liang,[†] Liang Hong,[‡] Hui Yang,[†] FeiFei Fan,[§] Yang Liu,[∥] Hong Li,[⊥] Ju Li,[#] Jian Yu Huang,[∥] Long-Qing Chen,[‡] Ting Zhu,[§] and Sulin Zhang*[,†]

[†]Department of Engineering Science and Mechanics, Pennsylvania State University, University Park, Pennsylvania 16802, United States

[‡]Department of Materials Science and Engineering, Pennsylvania State University, University Park, Pennsylvania 16802, United States

[§]Woodruff School of Mechanical Engineering, Georgia Institute of Technology, Atlanta, Georgia 30332, United States

[∥]Center for Integrated Nanotechnologies, Sandia National Laboratories, Albuquerque, New Mexico 87185, United States

[⊥]Renewable Energy Laboratory, Institute of Physics, Chinese Academy of Sciences, Beijing, 100190, China

[#]Departments of Nuclear Science and Engineering and Materials Science and Engineering, Massachusetts Institute of Technology, Cambridge, Massachusetts 02139, United States

Supporting Information

ABSTRACT: The irreversible chemomechanical degradation is a critical issue in the development of high-capacity electrode materials for the next-generation lithium (Li)-ion batteries. Here we report the self-healing behavior of gallium nanodroplets (GaNDs) under electrochemical cycling at room temperature, observed with *in situ* transmission electron microscopy (TEM). During lithiation, the GaNDs underwent a liquid-to-solid phase transition, forming a crystalline phase (Li_xGa) with ~160% volume expansion. Owing to the uneven Li flow during lithiation, the fully lithiated GaNDs exhibited highly distorted morphologies. Upon delithiation, the reverse phase transition occurred, accompanied with the nucleation and growth of a nanosized void. After the GaNDs were fully delithiated, the nanovoid gradually annihilated. Our analysis, along with phase field modeling and experimental measurements of the void growth and annihilation, provides mechanistic insights into the void formation and annihilation mechanism. The GaNDs may function as an effective healing agent in durable composite electrodes for high-performance Li-ion batteries, wherein active components, such as Si, are susceptible to fracture.

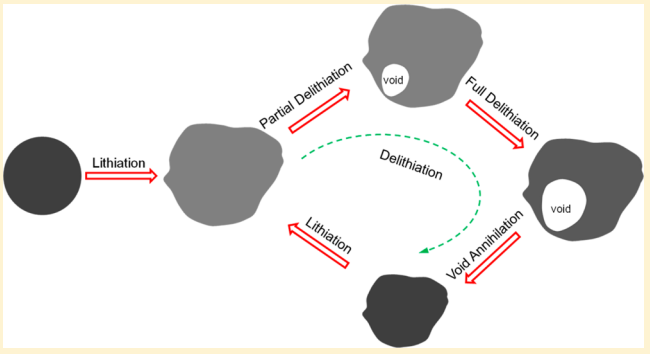

KEYWORDS: *Gallium nanodroplets, lithium ion battery, nanovoid, in situ TEM, phase field*

The demand for high-performance lithium (Li)-ion batteries (LIBs)[1−6] has led to intensive search for high-capacity materials to replace[7−13] carbonaceous electrodes in the current battery technology. However, commercialization of high-capacity electrodes, such as silicon (Si), has been hindered by their rapid, irreversible capacity decay and poor cyclability[10,13−16] due to the Li insertion/extraction induced huge volume changes and subsequent fracture. Nanostructured composite electrodes have been studied to mitigate the capacity fading.[14,17,18] Despite the rapid progress over the past few years, chemomechanical degradation of electrodes remains a serious issue in the development of next-generation LIBs. Gallium (Ga), a liquid metal at near room temperature, undergoes reversible liquid-to-solid transition during electrochemical lithiation/delithiation cycling.[19] For composites with active constituents (e.g., Si) that are susceptible to fracture,[14,20−22] liquid Ga may serve as a healing agent to fill and bond the cracked regions during delithiation.[19] Such self-healing composite electrodes may pave the way toward durable electrodes in high performance Li-ion batteries. Despite the promising application, the electrochemical cycling behavior of Ga remains unclear.

Here, we report the first in situ electrochemical tests on individual gallium droplets (GaNDs) using transmission electron microscopy (TEM).[23−28] Our real-time visualization revealed highly distorted morphological changes of GaNDs during lithiation, as well as nanovoid nucleation, growth, and annihilation during delithiation. We quantitatively measured the time laws of both nanovoid growth and annihilation. A phase field model[29] was also developed to elucidate the

Received: July 17, 2013
Revised: September 25, 2013
Published: October 8, 2013

   dx.doi.org/10.1021/nl402644w | *Nano Lett.* 2013, 13, 5212−5217

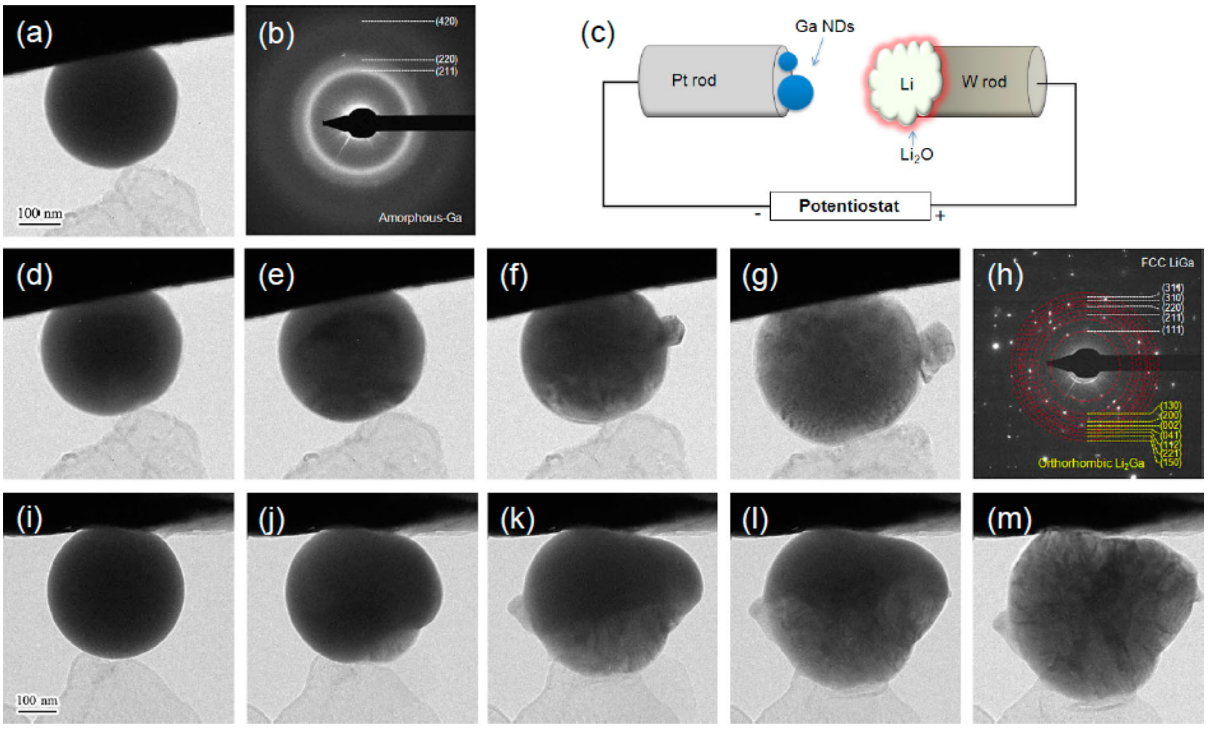

Figure 1. Phase transformation and morphological change of two GaNDs during lithiation. (a) A GaND with a diameter of ~335 nm. (b) The EDP indicates the GaND is amorphous. (c) Schematic illustration of the in situ nanobattery setup, consisting of a single GaND as the working electrode, bulk Li metal as the counter electrode, and a naturally grown Li_2O surface layer as the solid electrolyte. (d–g) TEM snapshots showing the distorted morphological evolution of the GaND. (d) The GaND was nearly uniformly lithiated, producing a lithiated shell–unlithiated core structure. (e) Uneven Li flow started to occur, with a faster Li flow on the bottom part than the upper part. (f) The liquid Ga was lithiated on its way of being squeezed out by the expanding lithiated part of the GaND, forming an extrusion at the upper-right corner. (g) Fully lithiated GaND underwent ~160% volume expansion compared to its initial size. (h) The EDP indicates the lithiated GaND is a composite crystal consisting of LiGa and Li_2Ga. (i–m) TEM snapshots showing the morphological evolution of a second GaND with a diameter of ~370 nm. (i) The GaND brought into contact with the Li_2O/Li electrode. (j–l) Lithiation started first from the lower side of the GaND and gradually propagated to the other size, yielding a clear visible lithiation front separating the lithiation and unlithiated regions. (m) Fully lithiated and crystallized phases.

mechanisms governing the void nucleation and growth morphology in the GaNDs during the delithiation process.

GaNDs were prepared by immersing a small piece of pure bulk Ga into ethanol solution, followed by sonication for about 30 min at 40 °C. Since the melting point of pure Ga is ~29 °C,[30] the bulk Ga was melted into nanometer-sized droplets with diameters ranging from 100 to 600 nm after sonication. A platinum (Pt) rod of 0.33 mm in diameter was then immersed into the solution, and the as-prepared, dispersed GaNDs attached on the flat end of the Pt rod. Figure 1a and i show two typical GaNDs with nearly perfect spherical shape, whose rounding behavior is presumably driven by the isotropic surface energy. The electron diffraction pattern (EDP) in Figure 1b confirmed that the as-prepared GaNDs were amorphous, denoted by *a*-Ga. To study the lithiation-delithiation cycling behavior of the GaNDs, an electrochemical device suited for in situ TEM experiment was constructed, as schematically shown in Figure 1c. The device consisted of three essential components: a single GaND as the working electrode attached on the Pt rod, a small piece of bulk Li metal as the counter electrode, and a native Li oxide (Li_2O) layer on the Li metal as the solid electrolyte.[14,25−27] All of the electrochemical tests were conducted inside a TEM operated at 300 kV with a Nanofactory TEM-scanning tunneling microscopy (STM) holder. Such an in situ TEM study enables real-time imaging of electrochemical reactions in individual nanoparticles and nanowires during lithiation–delithiation cycling.

Lithiation. To initiate lithiation, a negative bias −2 V was applied to the GaND working electrode with respect to the Li metal reference electrode. Figures 1d–g and i–m show the morphological evolution of two GaNDs during the first lithiation process. Both GaNDs had roughly the same initial size (~335 and 370 nm in diameter) but underwent different deformation modes upon lithiation. The first GaND (Figure 1a and d–g) expanded radially in a uniform manner in the initial lithiation stage. The lithiated and unlithiated regions formed a liquid core and solid shell structure, clearly distinguishable from the achromatic contrast. Similar core–shell structures have been observed in the lithiated Si and germanium (Ge) nanoparticles and nanowires.[31−33] The EDP in Figure 1h identified that the lithiated product is a LiGa/Li_2Ga composite in a solid crystalline phase,[19,30] denoted by *c*-Li_xGa. As lithiation proceeded, radial Li flow from the lower part of the GaND (on the side of the solid electrolyte) to the center appeared to be faster than from the upper part (on the side of the Pt substrate). The uneven inward Li flow broke the lithiation symmetry. As a result, the unlithiated core started to deviate from the circular shape (see Movie_S1 and Movie_S2 in the Supporting Information). Compressive stress is expected to generate near the lithiation reaction front owing to large volume expansion.[22,34,35] However, the nearly incompressible unlithiated liquid core pushes out the newly produced materials behind the lithiation reaction front, generating large loop tension in the surface layer of the lithiated shell and driving the

dx.doi.org/10.1021/nl402644w | *Nano Lett.* 2013, 13, 5212–5217

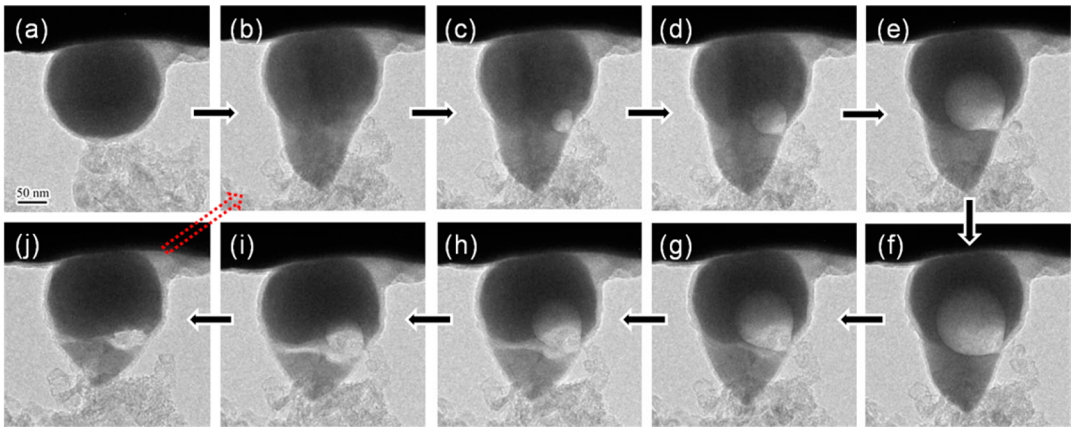

Figure 2. Void nucleation, growth, and annihilation of a GaND (~202 nm in diameter) during multiple cycling. (a) The pristine amorphous GaND in a spherical shape. (b) Lithiation induced the expansion of the GaND that deviated from the spherical shape. (c) A void nucleated at the beginning of delithiation. (d–f) The void grew during further delithiation. (f–j) The void gradually shrunk and finally disappeared after the GaND was fully delithiated.

formation and propagation of surface cracks.[27,34,35] The cracks subsequently relax the tension in the lithiated shell, creating a pressure difference between the lithiated shell and unlithiated core. The pressure difference drives the outward flow of the liquid Ga as a way of relaxing the compressive energy of the liquid Ga core (see Movie_S1 and Movie_S2 in the Supporting Information), wherein the cracks function as flow channels. The liquid Ga was fast lithiated on its way of being squeezed out and became a solid extrusion, as shown in Figure 1f and g. The fully lithiated GaND underwent ~160% volume expansion[30] compared to its initial size.

For the second GaND (Figure 1i–m), uneven Li flow occurred at the beginning of lithiation. The side near the Li metal fast lithiated, leaving the opposite side nearly intact. This indicates that the Li diffusivity at the GaND surface is probably comparable to that in the bulk of the liquid Ga phase, in distinct contrast to other anode materials such as Si[14] and Ge[27,31] in which lithiation always occurs first on the surface because of much larger Li diffusivity on their surface than in the bulk. As lithiation continued, the lithiation front in the GaND gradually propagated toward the other side, giving rise to a clearly visible interface between the lithiated solid phase and unlithiated liquid phase (see Movie_S1 and Movie_S2 in the Supporting Information). Due to the constraining effect of the Pt substrate and the solid electrolyte to the lithiation induced volume expansion, the unlithiated liquid portion of the GaND was compressed to a flattened shape. We observed that such uneven Li flow induced irregular morphologies were common in the lithiation of GaNDs. While it remains to be explored as to the exact mechanism that triggers the uneven Li flow,[36−38] the details of the geometrical constraints and of the contact condition between the GaND and the Li metal may play a critical role in the coupled lithiation–deformation process.

Delithiation. Figure 2 shows a lithiation–delithiation cycle of another GaND with a diameter of ~202 nm, with a focus on the delithiation process. During lithiation, the GaND could not maintain its spherical shape (Figure 2a) due to the aforementioned uneven radial Li flow and constraining effects. The fully lithiated GaND consisted of a conical extrusion at the side of the solid electrolyte, resembling a water droplet dripping from a ceiling (Figure 2b). To initiate delithiation, a bias +3 V was applied to the lithiated GaND with respect to the Li metal reference electrode. Due to the electrochemical Li extraction, the reverse phase transition from the solid (c-Li_xGa) to liquid (a-Ga) occurred. Figure 2d–f shows the TEM snapshots during the delithiation process. Interestingly, as Li started to be extracted, a nanovoid nucleated at the contact point of the GaND to the solid electrolyte (Figure 2c). The void expanded as delithiation continued (Figure 2d–e), reaching a maximal size when the GaND was fully delithiated (Figure 2f). The void shape slightly deviates from a circular shape with a higher curvature at the contact point to the solid electrolyte, much like the shape of a blowing balloon. After the GaND was fully delithiated and returned to its liquid amorphous phase, we held the delithiation conditions unchanged. The nanovoid gradually shrunk and finally disappeared (Figure 2g–j).

Subsequent lithiation-delithiation cycles were also studied for the GaND. Similar to the first cycle shown in Figure 2 (see Movie_S3, Movie_S4, and Movie_S5 in the Supporting Information), the distorted morphologies during lithiation and the void nucleation, growth, and annihilation during delithiation repeated periodically. Throughout the multiple cycling, the GaND was able to maintain its material integrity, despite void nucleation and growth, and progressively increased morphological distortion. It should be noted that, in Figure 2j, a crack-like defect appeared, separating the extruded area emerged at the lithiation process from the main GaND body. The crack-like defect was possibly due to the pulling force exerted by the Pt substrate and the solid electrolyte, which constrained the shrinkage of the GaND during delithiation. The crack gradually healed as the solid electrolyte moved closer to the substrate in the following lithiation–delithiation cycles.

Understanding the Nanovoid Formation and Annihilation. To utilize Ga as a self-healing agent in failure-resistant composite electrodes, it is essential to understand the lithiation–delithiation mechanism, as well as the dynamic morphological evolution, during electrochemical cycling. Here, we focus on a key experimental observation of nanovoid nucleation and growth during the delithiation of c-Li_xGa, which involves a multiscale process of local selective dealloying and long-range transport of Li. Specifically, the contact point between the lithiated GaND and the solid electrolyte acts as a sink to drive the outward flow of Li. As delithiation initiates, the electrochemical extraction of Li starts from the contact point and propagates toward the remote end of the GaND. The nanovoid nucleates and grows with continued Li extraction.

dx.doi.org/10.1021/nl402644w | Nano Lett. 2013, 13, 5212–5217

Currently, it remains unclear regarding the detailed spatial distribution of Ga and Li in the bulk phase outside the nanovoid, that is, whether there exists a two-phase or single-phase microstructure.[34,35,39,40] In the former, the nanovoid is enclosed by a Li-poor liquid-like layer that is further surrounded by the Li-rich solid-like bulk phase with a moving phase boundary between the two phases. In the latter, a smooth and gradual change of Li concentration exists in the bulk. In either case, the nanovoid grows until the GaND is fully delithiated, and the resultant nanovoid is surrounded by a pure liquid phase (a-Ga). Such delithiation mechanism through a single point sink is different from that observed in Si or Ge nanoparticles, where the entire surface effectively acts as a sink owing to the much higher Li diffusivity on the surface of Si and Ge than in the bulk.[14,20,27,31−33,35] Moreover, the development of a single major nanovoid in the delithiated GaND contrasts with the formation of distributed nanopores in the delithiated Ge nanowires (GeNWs).[31]

To further understand the underlying mechanisms of void nucleation and growth in GaNDs during the delithiation process, we developed a phase field model to simulate the dynamic formation and growth of the nanovoid.[41,42] Since our main purpose is to understand the shape evolution of the void, we assume that the bulk domain outside the nanovoid is a single Li-rich phase and the nanovoid is a Li-poor phase. A simple double-well function is used to represent the free energy functional governing the tempo-spatial Li distribution, with the mole fraction of Li denoted as $c(x;t)$ (see the Supporting Information). To mimic Li extraction, an outward Li flux J_n is specified at the contact point of the solid electrolyte and the GaND, normal to the GaND surface. The gradient term in our phase field formulation plays the role of surface tension for retaining the nearly circular shape of the nanovoid. In addition, we assume that the Li-poor phase is perfectly nonwetting to the Li-rich phase (see the Supporting Information), imposing a point contact of the nanovoid to the electrolyte, as observed in the experiment. Solving the Cahn−Hilliard diffusion equation with the specified boundary conditions produces the space and time evolution of the phase field variable $c(x; t)$ and thus the nucleation and growth morphology of the void.[43,44] Figure 3

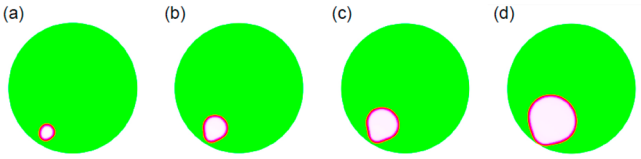

Figure 3. Phase field modeling of void nucleation and growth during the delithiation of GaND. The green region represents the matrix phase, the white region the void phase, and the red curve the interface. The void nucleation and morphologies resemble those seen in Figure 2.

displays four snapshots of the void nucleation and growth morphologies during the delithiation of the GaND. The outward Li flux is located at the left-bottom corner of the GaND, where the void nucleates. Our simulation demonstrated that the void shape is controlled by two competing effects: the rounding of the void surface to minimize surface area/energy and the local void expansion near the contact point driven by the Li outward flux. If the former is relatively fast, the void would be close to a circular shape. Oppositely, the void would deviate from the circular shape. With appropriately adjusted parameters, the simulated void expands like an inflated balloon with a necking region at the contact point to the solid electrolyte, which agrees with the experimentally observed morphologies.

To understand the annihilation of the nanovoid after full delithiation, it is important to appreciate the curvature effect on the chemical potential of surface atoms (or equivalently of free volumes). Geometrically, addition of an atom on the inner surface of a void *reduces* the void surface area by $2\Omega_A/r_{in}$, while that on the outer surface of a particle *increases* the particle surface area by $2\Omega_A/r_{out}$, where r_{in} and r_{out} denote the radius of a void and a particle, respectively, and Ω_A is the atomic volume. It follows that the chemical potential of an atom on the two surfaces is $\mu_{in} = \mu_0 - 2\gamma\Omega_A/r_{in}$ and $\mu_{out} = \mu_0 + 2\gamma\Omega_A/r_{out}$, respectively, where μ_0 is the chemical potential of an atom on a flat surface and γ is the surface energy per unit area. Since $\mu_{in} < \mu_{out}$, atoms tend to diffuse from the particle surface to the void surface, leading to the shrinkage and eventual annihilation of the void.

In addition to the focused study of the physical mechanisms and energetics governing the formation and annihilation of the nanovoid, we also measured the dynamic evolution of the nanovoid size from in situ TEM imaging. Figure 4 plots the

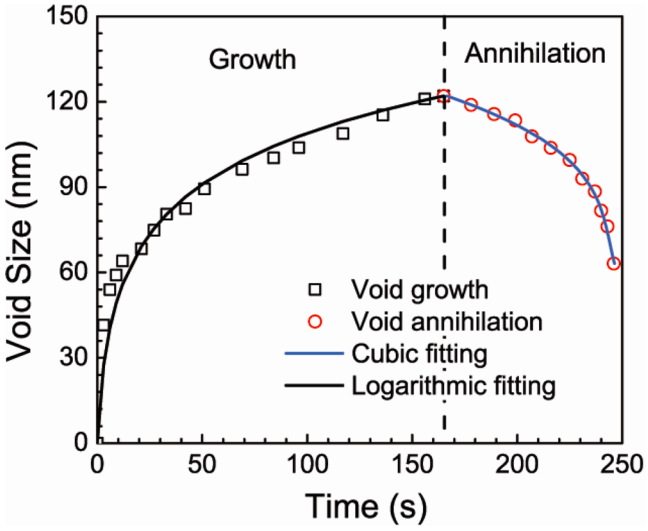

Figure 4. Nanovoid radius verse time (symbols) measured from in situ TEM experiment. The fitting curves (solid line) indicate that the void growth follows a logarithmic time law, while the annihilation follows a cubic time law.

void radius as a function of time for both void growth and shrinkage, exhibiting different time laws. We found that the void growth follows a logarithmic time law of $R = L_0 \ln(t/\tau + 1)$, with the fitting length constant $L_0 = 26.5$ nm and the time constant $\tau = 1.6$ s. The logarithmic growth has been often observed in thin film oxidation[45,46] at relatively low temperatures, where oxidation proceeds by oxygen invasion through pathways of connected leakage points, in contrast to the parabolic[47] growth controlled by diffusion. The logarithmic time growth could also be attributed to the leakage paths formed by connected free volumes from the delithiation front to the void surface, where the length of the leakage path increases as lithiation proceeds. A similar logarithmic time law was observed in the propagation of the nanoporous region during delithiation of GeNWs.[31] Figure 4 also shows that void

dx.doi.org/10.1021/nl402644w | Nano Lett. 2013, 13, 5212−5217

annihilation follows a cubic time law: $t \sim r_{in}^3$. The void size decreases slowly at the beginning of annihilation, but sharply in the late stage. Recall that the thermodynamic driving force of void annihilation can be attributed to the curvature effect on the chemical potential of surface atoms (or equivalently of free volumes). Along the same line, the cubic time law can be derived. As shown in the Supporting Information, this scaling law implies that the kinetic void annihilation is rate-limited by the diffusion of the free volume in the shell between the void and the GaND surface.

In summary, our in situ TEM studies demonstrated the dynamic morphological changes in GaNDs during electrochemical lithiation−delithiation cycling. During lithiation, the uneven Li flow during lithiation, likely triggered by the geometrical constraints, leads to irregular morphologies of the fully lithiated GaNDs. During delithiation, our experiments revealed the self-healing behavior of GaNDs by showing the nucleation, growth, and annihilation of a nanovoid. Our phase field modeling and theoretical analysis unraveled the void growth and annihilation mechanisms as well as the associated time laws. The reversible liquid-to-solid phase transition of Ga may enable a composite design of failure-resistant electrodes consisting of Ga as the self-healing agent and other active materials such as Si.

■ ASSOCIATED CONTENT

Supporting Information

Supporting movies (.mov) showing the lithiation/delithiation behaviors of GaNDs, a detailed description and figures of phase field modeling and the time law of void annihilation. This material is available free of charge via the Internet at http://pubs.acs.org.

■ AUTHOR INFORMATION

Corresponding Author

*E-mail: suz10@psu.edu.

Notes

The authors declare no competing financial interest.

■ ACKNOWLEDGMENTS

We acknowledge the support by National Science Foundation under the grant numbers CMMI-1201058, CMMI-1100205, CMMI-1235092, DMR-1240933 and DMR-1120901. Portions of this work were supported by a Laboratory Directed Research and Development (LDRD) project at Sandia National Laboratories (SNL) and partly by Nanostructures for Electrical Energy Storage (NEES), an Energy Frontier Research Center (EFRC) funded by the U.S. Department of Energy, Office of Science, Office of Basic Energy Sciences under Award Number DESC0001160. The LDRD supported the development and fabrication of platforms. The NEES center supported the development of TEM techniques. CINT supported the TEM capability; in addition, this work represents the efforts of several CINT users, primarily those with affiliation external to Sandia National Laboratories. In addition, this work was performed, in part, at the Sandia-Los Alamos Center for Integrated Nanotechnologies (CINT), a U.S. Department of Energy, Office of Basic Energy Sciences user facility. Sandia National Laboratories is a multiprogram laboratory operated by Sandia Corporation, a wholly owned subsidiary of Lockheed Martin Corporation, for the U.S. Department of Energy's National Nuclear Security Administration under contract DE-AC04-94AL85000.

■ REFERENCES

(1) Tarascon, J. M.; Armand, M. Issues and challenges facing rechargeable lithium batteries. *Nature* **2001**, *414* (6861), 359−367.

(2) Whittingham, M. S. Materials challenges facing electrical energy storage. *MRS Bull.* **2008**, *33* (4), 411−419.

(3) Goodenough, J. B.; Kim, Y. Challenges for Rechargeable Li Batteries. *Chem. Mater.* **2010**, *22* (3), 587−603.

(4) Tarascon, J. M. Key challenges in future Li-battery research. *Philos. Trans. R. Soc.* **2010**, *368* (1923), 3227−3241.

(5) Nazri, G. A.; Pistoia, G. *Lithium Batteries: Science and Technology*; Kluwer Academic Publishers: Boston, MA, 2003.

(6) Huggins, R. *Advanced batteries: materials science aspects*; Springer: New York, NY, 2009.

(7) Beaulieu, L. Y.; Eberman, K. W.; Turner, R. L.; Krause, L. J.; Dahn, J. R. Colossal reversible volume changes in lithium alloys. *Electrochem. Solid-State Lett.* **2001**, *4* (9), A137−A140.

(8) Limthongkul, P.; Jang, Y. I.; Dudney, N. J.; Chiang, Y. M. Electrochemically-driven solid-state amorphization in lithium-silicon alloys and implications for lithium storage. *Acta Mater.* **2003**, *51* (4), 1103−1113.

(9) Graetz, J.; Ahn, C. C.; Yazami, R.; Fultz, B. Nanocrystalline and thin film germanium electrodes with high lithium capacity and high rate capabilities. *J. Electrochem. Soc.* **2004**, *151* (5), A698−A702.

(10) Chan, C. K.; Peng, H.; Liu, G.; McIlwrath, K.; Zhang, X. F.; Huggins, R. A.; Cui, Y. High-performance lithium battery anodes using silicon nanowires. *Nat. Nanotechnol.* **2008**, *3* (1), 31−35.

(11) Zhang, W.-J. A review of the electrochemical performance of alloy anodes for lithium-ion batteries. *J. Power Sources* **2011**, *196* (1), 13−24.

(12) Marom, R.; Amalraj, S. F.; Leifer, N.; Jacob, D.; Aurbach, D. A review of advanced and practical lithium battery materials. *J. Mater. Chem.* **2011**, *21* (27), 9938−9954.

(13) Kamali, A. R.; Fray, D. J. Review on Carbon and Silicon Based Materials as Anode Materials for Lithium Ion Batteries. *J. New Mater. Electrochem. Syst.* **2010**, *13* (2), 147−160.

(14) Liu, X. H.; Zheng, H.; Zhong, L.; Huan, S.; Karki, K.; Zhang, L. Q.; Liu, Y.; Kushima, A.; Liang, W. T.; Wang, J. W.; Cho, J.-H.; Epstein, E.; Dayeh, S. A.; Picraux, S. T.; Zhu, T.; Li, J.; Sullivan, J. P.; Cumings, J.; Wang, C.; Mao, S. X.; Ye, Z. Z.; Zhang, S.; Huang, J. Y. Anisotropic Swelling and Fracture of Silicon Nanowires during Lithiation. *Nano Lett.* **2011**, *11* (8), 3312−3318.

(15) Neumann, G.; Würsig, A. Lithium storage in silicon. *Phys. Status Solidi RRL* **2010**, *4* (1−2), A21−A23.

(16) Lee, S. W.; McDowell, M. T.; Berla, L. A.; Nix, W. D.; Cui, Y. Fracture of crystalline silicon nanopillars during electrochemical lithium insertion. *Proc. Natl. Acad. Sci. U.S.A.* **2012**, *109* (11), 4080−4085.

(17) Goldman, J. L.; Long, B. R.; Gewirth, A. A.; Nuzzo, R. G. Strain Anisotropies and Self-Limiting Capacities in Single-Crystalline 3D Silicon Microstructures: Models for High Energy Density Lithium-Ion Battery Anodes. *Adv. Funct. Mater.* **2011**, *21* (13), 2412−2422.

(18) Yao, Y.; McDowell, M. T.; Ryu, I.; Wu, H.; Liu, N.; Hu, L.; Nix, W. D.; Cui, Y. Interconnected Silicon Hollow Nanospheres for Lithium-Ion Battery Anodes with Long Cycle Life. *Nano Lett.* **2011**, *11* (7), 2949−2954.

(19) Deshpande, R. D.; Li, J. C.; Cheng, Y. T.; Verbrugge, M. W. Liquid Metal Alloys as Self-Healing Negative Electrodes for Lithium Ion Batteries. *J. Electrochem. Soc.* **2011**, *158* (8), A845−A849.

(20) Liu, X. H.; Zhong, L.; Huang, S.; Mao, S. X.; Zhu, T.; Huang, J. Y. Size-Dependent Fracture of Silicon Nanoparticles During Lithiation. *ACS Nano* **2012**, *6* (2), 1522−1531.

(21) Lee, S. W.; McDowell, M. T.; Choi, J. W.; Cui, Y. Anomalous Shape Changes of Silicon Nanopillars by Electrochemical Lithiation. *Nano Lett.* **2011**, *11* (7), 3034−3039.

(22) Zhao, K.; Pharr, M.; Hartle, L.; Vlassak, J. J.; Suo, Z. Fracture and debonding in lithium-ion batteries with electrodes of hollow core−shell nanostructures. *J. Power Sources* **2012**, *218* (0), 6−14.
(23) Liu, X. H.; Liu, Y.; Kushima, A.; Zhang, S.; Zhu, T.; Li, J.; Huang, J. Y. In Situ TEM Experiments of Electrochemical Lithiation and Delithiation of Individual Nanostructures. *Adv. Energy Mater.* **2012**, *2* (7), 722−741.
(24) Huang, J. Y.; Zhong, L.; Wang, C. M.; Sullivan, J. P.; Xu, W.; Zhang, L. Q.; Mao, S. X.; Hudak, N. S.; Liu, X. H.; Subramanian, A.; Fan, H.; Qi, L.; Kushima, A.; Li, J. In Situ Observation of the Electrochemical Lithiation of a Single SnO_2 Nanowire Electrode. *Science* **2010**, *330* (6010), 1515−1520.
(25) Liu, X. H.; Huang, J. Y. In situ TEM electrochemistry of anode materials in lithium ion batteries. *Energy Environ. Sci.* **2011**, *4* (10), 3844−3860.
(26) Liu, Y.; Zheng, H.; Liu, X. H.; Huang, S.; Zhu, T.; Wang, J.; Kushima, A.; Hudak, N. S.; Huang, X.; Zhang, S.; Mao, S. X.; Qian, X.; Li, J.; Huang, J. Y. Lithiation-Induced Embrittlement of Multiwalled Carbon Nanotubes. *ACS Nano* **2011**, *5* (9), 7245−7253.
(27) Liang, W. T.; Yang, H.; Fan, F. F.; Liu, Y.; Liu, X. H.; Huang, J. Y.; Zhu, T.; Zhang, S. L. Tough Germanium Nanoparticles under Electrochemical Cycling. *ACS Nano* **2013**, *7* (4), 3427−3433.
(28) Wang, C.-M.; Xu, W.; Liu, J.; Zhang, J.-G.; Saraf, L. V.; Arey, B. W.; Choi, D.; Yang, Z.-G.; Xiao, J.; Thevuthasan, S.; Baer, D. R. In Situ Transmission Electron Microscopy Observation of Microstructure and Phase Evolution in a SnO2 Nanowire during Lithium Intercalation. *Nano Lett.* **2011**, *11* (5), 1874−1880.
(29) Chen, L. Q. Phase-field models for microstructure evolution. *Annu. Rev. Mater. Res.* **2002**, *32*, 113−140.
(30) Saint, J.; Morcrette, M.; Larcher, D.; Tarascon, J. M. Exploring the Li−Ga room temperature phase diagram and the electrochemical performances of the Li_xGa_y alloys vs. Li. *Solid State Ionics* **2005**, *176* (1−2), 189−197.
(31) Liu, X. H.; Huang, S.; Picraux, S. T.; Li, J.; Zhu, T.; Huang, J. Y. Reversible Nanopore Formation in Ge Nanowires during Lithiation-Delithiation Cycling: An In Situ Transmission Electron Microscopy Study. *Nano Lett.* **2011**, *11* (9), 3991−3997.
(32) Wang, C.-M.; Li, X.; Wang, Z.; Xu, W.; Liu, J.; Gao, F.; Kovarik, L.; Zhang, J.-G.; Howe, J.; Burton, D. J.; Liu, Z.; Xiao, X.; Thevuthasan, S.; Baer, D. R. In Situ TEM Investigation of Congruent Phase Transition and Structural Evolution of Nanostructured Silicon/Carbon Anode for Lithium Ion Batteries. *Nano Lett.* **2012**, *12* (3), 1624−1632.
(33) McDowell, M. T.; Ryu, I.; Lee, S. W.; Wang, C.; Nix, W. D.; Cui, Y. Studying the Kinetics of Crystalline Silicon Nanoparticle Lithiation with In Situ Transmission Electron Microscopy. *Adv. Mater.* **2012**, *24* (45), 6034−6041.
(34) Huang, S.; Fan, F.; Li, J.; Zhang, S.; Zhu, T. Stress generation during lithiation of high-capacity electrode particles in lithium ion batteries. *Acta Mater.* **2013**, *61* (12), 4354−4364.
(35) Yang, H.; Huang, S.; Huang, X.; Fan, F.; Liang, W.; Liu, X. H.; Chen, L.-Q.; Huang, J. Y.; Li, J.; Zhu, T.; Zhang, S. Orientation-Dependent Interfacial Mobility Governs the Anisotropic Swelling in Lithiated Silicon Nanowires. *Nano Lett.* **2012**, *12* (4), 1953−1958.
(36) Yang, H.; Huang, X.; Liang, W.; van Duin, A. C. T.; Raju, M.; Zhang, S. Self-weakening in lithiated graphene electrodes. *Chem. Phys. Lett.* **2013**, *563* (0), 58−62.
(37) Liu, X. H.; Fan, F.; Yang, H.; Zhang, S.; Huang, J. Y.; Zhu, T. Self-Limiting Lithiation in Silicon Nanowires. *ACS Nano* **2013**, *7* (2), 1495−1503.
(38) Grantab, R.; Shenoy, V. B. Pressure-Gradient Dependent Diffusion and Crack Propagation in Lithiated Silicon Nanowires. *J. Electrochem. Soc.* **2012**, *159* (5), A584−A591.
(39) McDowell, M. T.; Lee, S. W.; Harris, J. T.; Korgel, B. A.; Wang, C.; Nix, W. D.; Cui, Y. In Situ TEM of Two-Phase Lithiation of Amorphous Silicon Nanospheres. *Nano Lett.* **2013**, *13* (2), 758−764.
(40) Wang, J. W.; He, Y.; Fan, F.; Liu, X. H.; Xia, S.; Liu, Y.; Harris, C. T.; Li, H.; Huang, J. Y.; Mao, S. X.; Zhu, T. Two-Phase Electrochemical Lithiation in Amorphous Silicon. *Nano Lett.* **2013**, *13* (2), 709−715.
(41) Yu, H.-C.; Chen, H.-Y.; Thornton, K. Extended smoothed boundary method for solving partial differential equations with general boundary conditions on complex boundaries. *Modell. Simul. Mater. Sci. Eng.* **2012**, *20* (7), 075008.
(42) Bueno-Orovio, A.; Perez-Garcia, V. M.; Fenton, F. H. Spectral methods for partial differential equations in irregular domains: The spectral smoothed boundary method. *SIAM J. Sci. Comput.* **2006**, *28* (3), 886−900.
(43) Granasy, L.; Pusztai, T.; Saylor, D.; Warren, J. A. Phase field theory of heterogeneous crystal nucleation. *Phys. Rev. Lett.* **2007**, *98* (3), 035703.
(44) Warren, J. A.; Pusztai, T.; Kornyei, L.; Granasy, L. Phase field approach to heterogeneous crystal nucleation in alloys. *Phys. Rev. B* **2009**, *79* (1), 014204.
(45) Davies, D. E.; Evans, U. R.; Agar, J. N. The Oxidation of Iron at 175 to 350 degrees C. *Proc. R. Soc. A* **1954**, *225*, 443−462.
(46) Lawless, K. R. The oxidation of metals. *Rep. Prog. Phys.* **1974**, *37*, 231−316.
(47) Deal, B. E.; Grove, A. S. General Relationship for the Thermal Oxidation of Silicon. *J. Appl. Phys.* **1965**, *36* (12), 3770−3778.

Supporting Information

Nanovoid Formation and Annihilation in Gallium Nanodroplets under Lithiation-Delithiation Cycling

Wentao Liang,[†] Liang Hong,[‡] Hui Yang,[†] FeiFei Fan,[§] Yang Liu,[¶] Hong Li,[◊] Ju Li,[⊥] Jian Yu Huang,[¶] Long-Qing Chen,[‡] Ting Zhu,[§] and Sulin Zhang[†,1]

[†]Department of Engineering Science and Mechanics, Pennsylvania State University, University Park, Pennsylvania 16802, United States

[‡]Department of Materials Science and Engineering, Pennsylvania State University, University Park, Pennsylvania 16802, United States

[§]Woodruff School of Mechanical Engineering, Georgia Institute of Technology, Atlanta, Georgia 30332, United States

[¶]Center for Integrated Nanotechnologies, Sandia National Laboratories, Albuquerque, New Mexico 87185, United States

[◊]Renewable Energy Laboratory, Institute of Physics, Chinese Academy of Sciences, Beijing, 100190, China

[⊥]Departments of Nuclear Science and Engineering and Materials Science and Engineering, Massachusetts Institute of Technology, Cambridge, Massachusetts 02139, United States

I. Phase Field Modeling

Our phase field model employs the tempo-spatial Li distribution $c(\boldsymbol{x}; t)$ as the order parameter to illustrate the void nucleation and growth in GaNDs during the delithiation process. Since our main purpose is to understand the shape evolution of the void, the present model considers a

[1]Corresponding Author: suz10@psu.edu

two-phase transition process, i.e. the void phase (Li-poor phase) with a small c and the matrix phase (Li-rich) with a large c which is composed of lithiated solid and delithiated liquid (between void and solid) phases. Figure S1 gives the schematic of the present phase-field model.

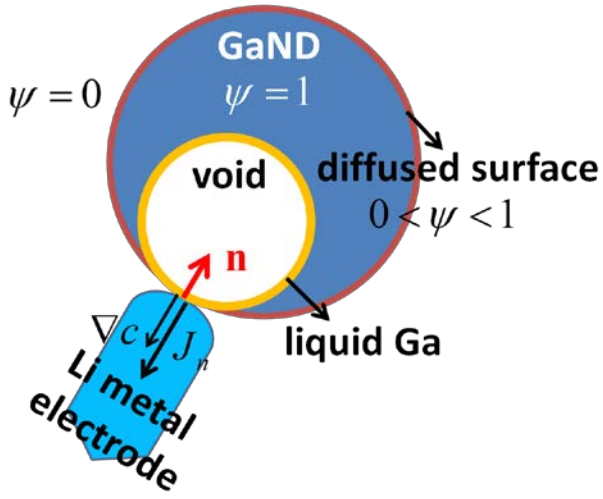

Figure S1. Schematic of the phase-field model implemented through spectral smoothed boundary method.

The total free energy of the system is composed of the chemical energy and gradient energy,

$$F_{tot} = \int_V \left[f_{chem}(c,T) + f_{gra}(\nabla c) \right] dV \,, \tag{1}$$

Here the chemical energy is expressed with regular solution formulation,

$$f_{chem}(c,T) = N_v \left[\Lambda c(1-c) + kT\left(c\ln c + (1-c)\ln(1-c) \right) \right], \tag{2}$$

where N_v is the number of atoms per unit volume, Λ is the regular solution parameter, k is the Boltzmann constant, T is the absolute temperature. This double-well chemical energy function as shown in Figure S2 produces two stable phases. The gradient energy

$$f_{gra}(\nabla c) = \frac{\lambda}{2}(\nabla c)^2 \tag{3}$$

represents the penalty energy whenever an interface is introduced, where λ is the gradient coefficient. The Cahn-Hilliard diffusion equation is used to depict the void growth dynamics starting from the GaND-electrolyte contact point where an outward Li flux J_n is specified. The void nucleation is originated from that contact point and controlled by the heterogeneous nucleation process.[1, 2] During the delithiation process, the void is covered by and tangential to GaND surface, much like a non-wetting phase to the GaND. Therefore, a boundary condition with $\theta(\nabla c, \mathbf{n}) = \pi$ is applied to the phase interface on the particle surface to control the void morphology. Here $\mathbf{n} = \frac{\nabla \psi}{|\nabla \psi|}$ is the unit inward normal vector locating on the GaND surface, and $\mathbf{n} \cdot \nabla c = \sqrt{\frac{2\Delta f}{k}} \cos\theta$ where $\Delta f = f_{chem}(c) - f_{chem}^{\min}$ is the energy difference to the bulk chemical energy.[1, 3] Any deviation from this non-wetting boundary condition would lead to void spreading along the GaND surface as shown in Figure S3.

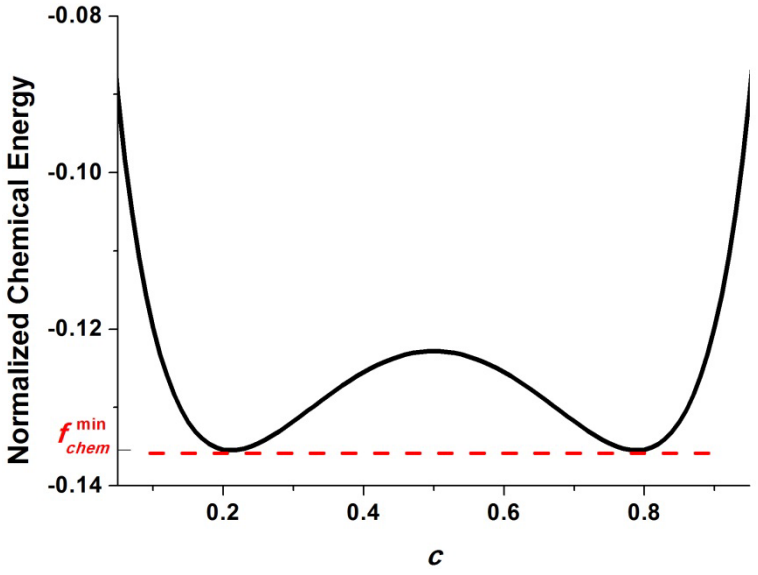

Figure S2. The variation of the normalized chemical energy to the Li distribution $c(\boldsymbol{x}; t)$ at room temperature.

Spectral smoothed boundary method,[3-5] which is able to solve the Cahn-Hilliard equation with the surface boundary conditions of arbitrary domain shape, is adopted in the present phase-field model. A domain parameter ψ, which has constant values inside or outside the GaND, but varies continuously across the diffused particle surface, is used to identify the GaND surface and apply the boundary conditions. The Cahn-Hilliard equation in the spectral smoothed boundary approach is written as,

$$\frac{\partial c}{\partial t} = \nabla \cdot (\mathbf{M} \nabla \mu) = \frac{1}{\psi} \nabla \cdot \left[\psi \mathbf{M} \nabla \left(\frac{\partial f_{chem}}{\partial c} - \frac{\lambda}{\psi} \nabla \cdot \left(\psi \nabla c \right) + \frac{\lambda}{\psi} \nabla \psi \cdot \nabla c \right) \right] + \frac{|\nabla \psi|}{\psi} J_n, \tag{4}$$

where $\mathbf{M}$ is the Li mobility whose value in the void phase is assumed to be ten times larger than that in the matrix phase. Notice that the two boundary conditions, i.e. the Li outward flux and the void contact behavior to GaND, have been incorporated into the above kinetic equation.

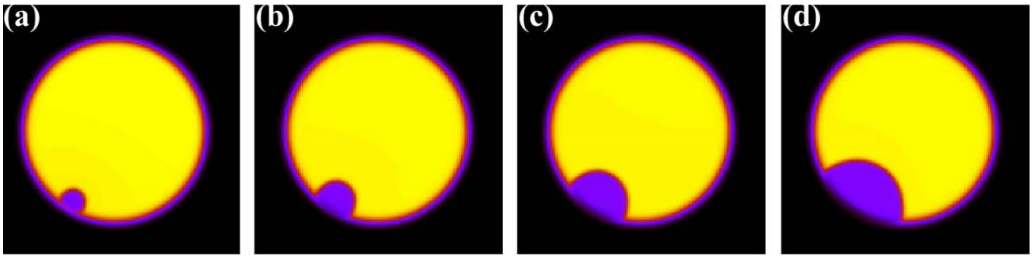

Figure S3. Void nucleation and growth with $\theta(\nabla c, \mathbf{n}) = \pi/2$.

The computational domain size is 128 Δx x128 Δy with domain parameter $\psi = 0.5 + 0.5\left(\tanh \frac{r_0 - r}{\varsigma} \right)$, where $r_0 = 40$, $\varsigma = 2.0$ and r measures the displacement of any grid position to the GaND center point. The free energy related parameters are obtained from ref. 6,[6] i.e. N_v=8.396×10^{28} m^{-3}, $\Lambda = 59$ meV, $T = 300$ k. Moreover, the normalized outward Li flux and gradient coefficient are equal to 0.02 and 0.4 respectively.

II. Time Law of Void Annihilation

Owing to the curvature effect described in the main text, the chemical potential of an atom (a free volume) is higher (lower) on GaND surface than on the void surface, atoms (free volumes) tend to diffuse from the outer (inner) to the inner (outer) surface, thus filling (annihilating) the void. To derive the time law of void annihilation along the same line of Tu and Gosele,[7] one expresses the local equilibrium concentration of the free volume as a function of the mean curvature $\bar{\kappa}$:

$$c(\bar{\kappa}) = c_0 e^{-\Delta\mu_F(\bar{\kappa})/kT}, \tag{5}$$

where $\Delta\mu_F(\bar{\kappa}) = 2\gamma\bar{\kappa}\Omega_V$ is the chemical potential difference of a free volume on the curved surface and a flat surface, c_0 is the local equilibrium concentration of free volume on a flat surface, γ is the surface energy per unit area, and Ω_F the volume of the free volume. Since $\left|\Delta\mu_F(\bar{\kappa})/kT\right| << 1$ typically holds, one has $c(\bar{\kappa}) \approx c_0\left(1-\Delta\mu_F(\bar{\kappa})/kT\right)$. On the void surface $\bar{\kappa} = 1/r_{\text{in}}$, while on the GaND outer surface $\bar{\kappa} = -1/r_{\text{out}}$ (The signs of the mean curvatures are defined such that they are consistent with those of the chemical potential energy differences). This follows that the local equilibrium concentration of free volume at the two surfaces is $c_{\text{in}} = c_0\left(1+\beta/r_{\text{in}}\right)$and $c_{\text{out}} = c_0\left(1-\beta/r_{\text{out}}\right)$, respectively, where $\beta = 2\gamma\Omega_F/kT$.

Assuming a steady state process and with the two boundary conditions prescribed by c_{in} and c_{out}, the concentration of free volume in the shell can be solved in a spherical coordinate system as:

$$c(r) = c_0\beta\frac{r_{\text{out}}+r_{\text{in}}}{r_{\text{out}}-r_{\text{in}}}\frac{1}{r} - c_0\beta\frac{2}{r_{\text{out}}-r_{\text{in}}} + c_0. \tag{6}$$

It follows that the flux of the free volume is

$$J_F = -D_F\frac{\mathrm{d}c}{\mathrm{d}r} = D_F c_0\beta\frac{r_{\text{out}}+r_{\text{in}}}{r_{\text{out}}-r_{\text{in}}}\frac{1}{r^2}, \tag{7}$$

where D_F is the diffusivity constant of the free volume. The rate of change of r_{in} is given by the geometrical relation at the inner surface:

$$\frac{dr_{in}}{dt} = -J_F\Big|_{r=r_{in}} \Omega_F, \tag{8}$$

Assuming $r_{in} \ll r_{out}$, one obtains an estimate of the time needed to fill the void

$$t \sim \frac{r_{in}^3}{D_F \Omega_F c_0 \beta}. \tag{9}$$

III. Supporting Movies

Movie_S1.mov, Movie_S2.mov

In situ TEM movies show the distorted morphological evolution of the GaNDs during lithiation. The videos were recorded at 3 frames/s and played at 5× (Movie_S1.mov) and 20× (Movie_S2.mov) speed.

Movie_S3.mov, Movie_S4.mov, Movie_S5

In situ TEM movies show the delithiation process with nanovoid nucleation, growth, and annihilation. Movie_S3.mov and Movie_S4.mov show the delithiation during the first and second cycles, respectively. Movie_S5 shows the delithiation of another GaND with the similar behavior. The videos were recorded at 3 frames/s and played at 10× speed.

References:

1. Granasy, L.; Pusztai, T.; Saylor, D.; Warren, J. A. Phase Field Theory of Heterogeneous Crystal Nucleation. *Phys. Rev. Lett.* **2007,** *98* (3), 035703.
2. Warren, J. A.; Pusztai, T.; Kornyei, L.; Granasy, L. Phase field approach to heterogeneous crystal nucleation in alloys. *Phys. Rev. B* **2009,** *79* (1), 014204.

3. Yu, H. C.; Chen, H. Y.; Thornton, K., Extended Smoothed Boundary Method for Solving Partial Differential Equations with General Boundary Conditions on Complex Boundaries. arXiv: 1107.5341 [math-ph] **2011**.
4. Hong, L.; Liang, L.; Bhattacharyya, S.; Xing, W.; Chen, L.-Q. To Be Submitted.
5. Bueno-Orovio, A.; Perez-Garcia, V.; Fenton, F. Spectral Methods for Partial Differential Equations in Irregular Domains: The Spectral Smoothed Boundary Method. *SIAMJ. Sci. Comput.* **2006,** *28* (3), 886-900.
6. Maxisch, T.; Ceder, G. Elastic properties of olivine LixFePO4 from first principles. *Phys. Rev. B* **2006,** *73* (17).
7. Tu, K. N.; Gosele, U. Hollow nanostructures based on the Kirkendall effect: Design and stability considerations. *Appl. Phys. Lett.* **2005,** *86* (9), 3.